Theor Chem Account (2009) 122:297–304
DOI 10.1007/s00214-009-0509-0

REGULAR ARTICLE

Bidimensionality of 8-atom clusters of Au: first principles study and comparison with Ag clusters

Jorge Botana · Manuel Pereiro · Daniel Baldomir · Juan Enrique Arias

Received: 22 October 2008 / Accepted: 7 January 2009 / Published online: 3 February 2009

Abstract We have calculated the lowest energy structures of 8-atom neutral gold clusters using the density functional theory approach. In contrast with current literature that finds kinetic energy to be the determinant component, we have found that the 2D structure is energetically favored due to a higher electron delocalization that stems from the relativistic contraction of Au atom size which cause 3D clusters to deform. This higher delocalization lowers the total energy of the 2D structures against the 3D ones. Silver clusters do not suffer this size contraction, hence there is no higher delocalization in the 2D clusters, and their fundamental structure will be 3D.

Keywords Small clusters · Gold clusters · Ab initio · DFT

1 Introduction

Within the current trends of the research in nanoscience, the development and study of structures with a low number of atoms (clusters and nanoparticles) has become a topic of major interest, where different fields of knowledge (Physics, Chemistry, Biomedicine and Engineering) converge. The noble metals Cu, Ag and Au, are the focus of much of this research. The Au clusters, particularly, show a widespread of very interesting properties that are being predicted: interaction and stabilization of DNA [1], relatively high magnetic moments [2], structure-dependent adsorption of amino-acids [3], role in organic catalysis [4–6] properties of molecules where they interact with sulfur [7, 8]. Most of these properties of Au clusters come from the low-dimensionality structures they conform, in contrast with Ag and Cu. It could be thought that Au, Ag and Cu, being isoelectronic, would play an interchangeable role in molecules or atomic aggregates. This is often the truth, especially when it comes to chemical properties. The clusters of these three elements adopt planar structures from 1- to 8-atom size. But, while Ag and Cu 8-atom clusters have been shown to adopt the geometry of a distorted bi-capped octahedron with symmetry D_{2d} [9, 10]. Ab initio calculations with pseudopotentials [9–13] and perturbative methods [14] have currently established that the 8-atom gold cluster is a tetracapped square with symmetry D_{4h}. Au clusters keep their 2D character up to 12 atoms: in this cluster, the lowest energy structure is already tridimensional. This late 2D–3D transition in the Au small clusters has attracted considerable attention [9–11, 15–17]. The reason why this happens is known to be the stronger relativistic effect Au atom electrons suffer. Previous works [9, 10, 16] find that this happens due to strong *d–d* orbitals overlap in the 2D structures, which makes them energetically competitive with respect to the 3D ones. The Ag and Cu clusters are less electronically dense and there will not be as much *d–d* overlap, hence the 2D structures will not be energetically favoured. Using a different approach, we show that the *d–d* overlap actually lowers the energy for 3D Au clusters, and the exchange-correlation (XC) and the electron–electron (*e–e*) repulsion favors 2D ones.

In the present paper we will compare our ab initio calculations on different structures for the 8-atom neutral

J. Botana (✉) · M. Pereiro · D. Baldomir
Departamento de Física Aplicada, Universidade de Santiago de Compostela, 15782 Santiago de Compostela, Spain
e-mail: jorge.botana@usc.es

J. Botana · M. Pereiro · D. Baldomir · J. E. Arias
Instituto de Investigacións Tecnolóxicas, Universidade de Santiago de Compostela, 15782 Santiago de Compostela, Spain

clusters of Au and Ag. From this comparison, we will try to deduce how Au clusters tend to arrange in 2D structures. In Sect. 2 we explain our computational method to perform the simulations. In Sect. 3 we show the results of our search for the lowest energy structure for Au_8 clusters, and compare it with the results obtained for Ag_8. In Sect. 4 we split the energy for the lowest-lying structures and look for the terms that favor either bidimensionality or tridimensionality. We also show our graphical results for the electron localization function (ELF) and the highest occupied molecular orbital (HOMO), together with the density of states (DOS). Finally, in Sect. 5 we present our analysis of the previous data and our conclusions.

2 Method and computational details

We have performed ab initio calculations within the frame of the density functional theory (DFT). We have solved each system using linear combinations of Gaussian-type orbitals within the Kohn–Sham density functional methodology (LCGTO–KSDFM), with the program deMon-ks3p5 [18]. The calculation of the XC energy term was carried out using the generalized gradient approximation (GGA), with the Perdew-Wang 91 parametrization [19] It has been shown that the GGA is the approximation that gives the best results for geometry optimizations of these small clusters [20, 21]. The orbital basis set used in our calculations [22] has the contraction pattern (22211/22211/221) for describing the outer 17 electrons: $5p^6$ $5d^{10}$ $6s^1$. Contraction pattern building rules can be found in the work by Godbout et al. [23] The core electrons are considered in a relativistic model-core potential with the contraction pattern (7:12,9,7,5), built according to Andzelm et al. work [24]. The electron density is expanded in the auxiliary basis set (5,5;5,5) in order to avoid the calculation of the N^4 scaling Coulomb repulsion energy, where N is the number of the basis functions.

We have calculated nine different geometries that can be seen in Fig. 1. They have been chosen from the structures

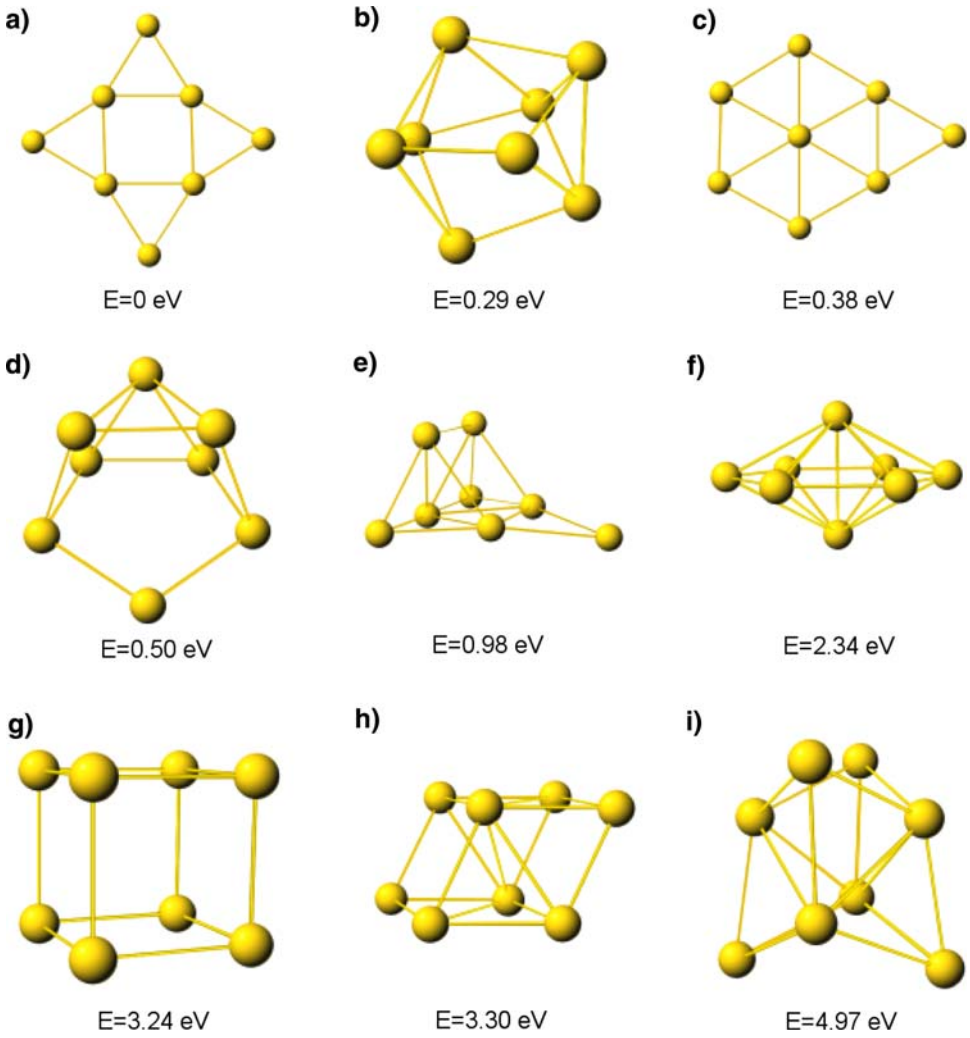

Fig. 1 Lowest energy structures of the gold 8-atom cluster according to our calculations are presented. Below each structure, we show the energy difference respect to the fundamental one, the D_{4h} tetra-capped square, in eV. Structures **a** and **c** are 2D, while the rest are 3D

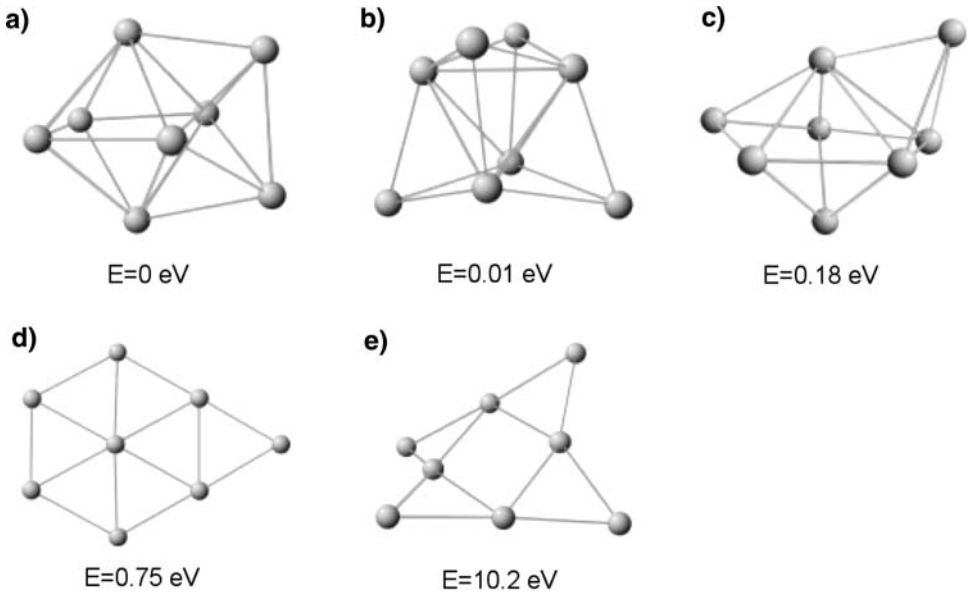

Fig. 2 **a–c** The three lower energy structures of the silver 8-atom cluster according to our calculations are presented. Below each structure, we show the energy difference respect to the fundamental one, the D_{2d} bi-capped octahedron, in eV. 2D structures **d** and **e** were added for comparison. It is to be noted how the **e** structure, originally a D_{4d} tetra-capped square is not stable as a purely bidimensional structure for silver

that are used in the literature for metallic clusters of 8 atoms, and other regular arrangements, like a cubic one and a fcc one. They all have had a first geometry optimization through a Born-Oppenheimer molecular dynamics simulation. After this first approach, the geometry of each cluster was optimized further with a Broyden–Fletcher–Goldfarb–Shanno algorithm [25]. Also, we carried out a search in the magnetic state that yields the energy minimum for zero external magnetic field and $T = 0$ for each geometry.

The search of the magnetic minimum state has been done between spin multiplicities 1 and 11, and it has been found to be one in every case. The chosen convergence criteria were, in atomic units: 10^{-7} for energy, 10^{-6} for electron density and 10^{-4} for the gradient. The *d* orbital components have been treated considering six Cartesian *d* functions: d_{XX}, d_{XY}, d_{XZ}, d_{YY}, d_{YZ}, d_{ZZ}. To facilitate convergence, we have allowed a small window of 0.15 eV around Fermi Energy where the occupation can be fractional. In the self-consistent field procedure, the input electron density for each iteration is directly mixed with the input electron density for the previous iteration. Our mixing factor was 0.05, reducing it as necessary to facilitate convergence. Between consecutive steps of the geometry optimization, the maximum possible average displacement of the atomic positions was set to 0.026 Å.

3 Geometry

After performing a geometry optimization in all our systems, we found that the global energy minimum happens for the tetracapped square. In Fig. 1 we report the energies (in eV) of every geometry respect to the minimum configuration. The 2D structure at Fig. 1a, a D_{4h} tetra-capped square, being minimum for the 8-atom Au cluster is a well-established fact by now [9, 10, 26]. The second lowest energy structure is a distorted form of the D_{2d} bi-capped octahedron (Fig. 1b), that is also (when undistorted) the energy minimum of Ag and Cu 8-atom clusters. The third structure is also 2D: a mono-capped hexagon with C_{2v} symmetry (Fig. 1c). The 4th lowest energy structure is 3D: a bi-capped octahedron with C_{2v} symmetry (Fig. 1d), which is distorted as well.

A remarkable trend is how the 3D structures are distorted. We start the convergence procedure of the calculation with a regular arrangement, and the final result is the distorted structure. This means that in Au 3D 8-atom clusters, the regular structures are not energetically favored against their distortions. Attempting to find a geometrical reason behind these distortions, we proceeded to analyze the average distance between first neighbor atoms, and the average coordination number in each cluster. Results are shown in Table 1.

We have found the following: the first neighbor distance is slightly larger in 3D cluster than in 2D ones (2.68 and 2.62 against 2.56 and 2.61 Å). Also, the distortions in the 3D clusters seem to reduce the average coordination number of their atoms: their coordination indices changes from 4.50 in the regular 3D structures to 3.75 and 3.00. Hence, we conclude that geometry optimization of 8-atom clusters tend to produce structures with a low coordination index, and large average distance among atom nuclei. This points toward a relaxation of the nuclear and *e–e* repulsion being energetically favorable, favoring hollow structures. An analogous behavior has been recently calculated for

Table 1 The value of different structural parameters of the four lowest energy structures of the 8-atom Au cluster are given

	(*a*)	(*b*)	(*c*)	(*d*)
coord	3.00	3.75	3.50	3.00
coord*	3.00	4.50	3.50	4.50
$\bar{d}$	2.56	2.68	2.61	2.62
$\bar{D}$	3.97	3.29	3.81	3.44

coord the average coordination index of each cluster, *coord** the average coordination number of the regular structure the cluster comes from (this parameter is significative for 3D clusters since they are strongly distorted). $\bar{d}$ the average distance among first neighbors, and $\bar{D}$ the average distance among all the cluster atoms. Distances are given in Å. Columns (a), (b), (c), (d) correspond to the a, b, c and d structures in Fig. 1

larger Au clusters (from 20 to 50 atoms) [27–29], but not for the smaller ones.

4 Electronic structure

In our previous work [30], we found that the structure that minimizes the energy of 8-atom Ag clusters is the bi-capped octahedron (Fig. 1a), and the second lowest structure is a tetra-capped tetrahedron with T_d symmetry (Fig. 1b). These results match with the minimum structures for Cu [10]. Both structures are almost degenerate with a difference of only 0.006 eV between them. The third lower local minimum, a capped pentagonal bi-pyramid with C_s symmetry, has a higher energy, 0.182 eV over the fundamental state. It is reported that the Cu lower energy structures are also found in a narrow energetic margin [9, 10]. In contrast, the differences between Au structures are wider: as we see in the Fig. 1, the five lower energy structures span over 1 eV.

We break down the total energy components in Table 2, and we calculate the differences between the energy terms of each cluster and the same energy component of the lowest energy structure (that is 2D). We have only included the energy terms that show a dependence on the dimensionality of the cluster. The kinetic energy (ΔE_K) component favors 3D structures: they lower the E_K by 37.30 and 38.58 eV respect to the global minimum isomer (which is 2D), and the other 2D cluster increases it by 3.26 eV. The kinetic energy is lowered by *d–d* orbital interaction [16] and tighter-packed 3D clusters will have stronger *d–d* interaction. In the 2D clusters, the (a) structure has a smaller distance between first neighbors than the (c) one (Fig. 1; Table 1) so it will have a smaller kinetic energy as well. The Coulomb (ΔE_C) interaction is opposite as the 3D clusters have it raised by 3,800 and 2,461 eV respect to the lowest-lying one, while the other 2D cluster raises it by only 1,008 eV. The XC energy term (ΔE_{XC})

Table 2 We present the energy of each one of the four lowest energy structures Au clusters from our calculations, the energy of the three lowest-lying structures for Ag and the energy of two 2D structures for Ag according to our calculations

Structure	ΔE_T	ΔE_K	ΔE_C	ΔE_{XC}
Au (a) 2D	0	0	0	0
Au (a) 3D	+0.29	−37.30	+3800	+2.06
Au (a) 2D	+0.38	+3.26	+1008	−0.13
Au (a) 3D	+0.50	−38.58	+2461	+2.74
Ag (a) 3D[a]	0	0	0	0
Ag (a) 3D[a]	+0.01	−7.00	−3462	+0.03
Ag (a) 3D[a]	+0.18	−1.03	−2522	+0.02
Ag (a) 2D	+0.75	+5.71	−32662	+0.36
Ag (a) 2D	+10.25	+56.71	−150955	+6.78

We only include the energy components that show a bias toward 2D or 3D isomers: The first column is the name of the structure according to Figs. 1 (for Au) and 2 (for Ag). Second column is the total energy of the clusters respect to the energy of the lowest-lying one. Following columns are the differences of the kinetic, Coulombian and exchange-correlation components of the energy respect to their value for the lowest-lying cluster. Energies are given in eV

[a] Results taken from Ref. [28]

favors 2D too: the increase is 2.06 and 2.74 eV in the 3D clusters, while in the other 2D cluster is reduced by 0.13 eV. Despite this, ΔE_K and ΔE_C differ by several orders of magnitude from the total energy difference respect to the global minimum cluster, ΔE_T. The ΔE_{XC} term shows the same bias as the total energy (favoring 2D structure) and is in a similar order of magnitude. Hence we conclude it is the ΔE_{XC} term the one that controls the preference small gold cluster has for planar structures.

In Table 2, we compare these results with our previous work for 3D silver clusters [30], plus two 2D silver clusters we calculated for this paper, which are the lowest energy 2D structures for gold. We only include the energy components that show a bias toward 2D or 3D isomers. For them, we keep observing the same trends as for Au clusters, regarding to the ΔE_K and ΔE_C. ΔE_{XC} is still the term that decides the minimum structure, but its importance is much lesser than in the Au. For Ag clusters, though, ΔE_{XC} favors 3D structures over 2D ones.

To understand where this comes from, and what it means, we will analyze the electronic localization in the clusters, as electron localization is related to the XC energy (see "Appendix"). The electron localization is not an observable; hence, it cannot be univocally defined. Because of this, there are available several theoretical methods to quantify it. In the present paper we adopt Becke and Edgecombe's definition [31], the ELF. In this definition and within the DFT framework, an increase of the electron delocalization corresponds with a reduction of the E_{XC},

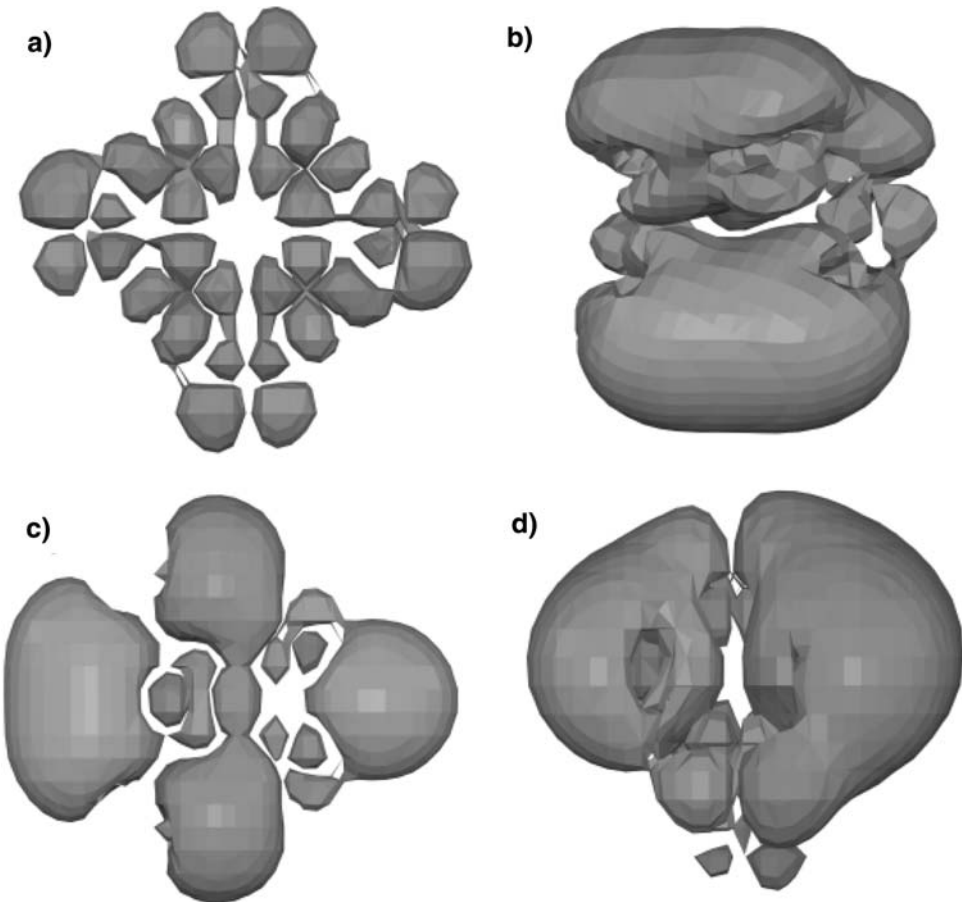

Fig. 3 The highest occupied molecular orbital (HOMO) is plotted for the four lowest energy structures of the 8-atom Au cluster. **a**–**d** are the HOMO of the **a**–**d** structures of Fig. 1, respectively. Isomers **a** and **c** are 2D, while **b** and **d** are 3D

whereas the opposite behavior is predicted for the E_{XC} if the localization increases. Electrons are perfectly localized for ELF = 1[1] and they are as delocalized as in a free-electron gas for ELF = 0.5. When the ELF takes values close to 0.5, it means that the electron delocalization is, consequently, fairly high. On the other hand, there is not a clear physical interpretation for ELF = 0, or close to zero. Taking this in account, we will show the HOMO and the ELF for the systems, in Figs. 3 and 4 respectively.

As shown in Fig. 3a, the HOMO of the (a) structure does not accumulate around any particular atom. Instead, the orbital takes the same shape for each of the atoms, as it is predominantly *d*, highly delocalized. In Fig. 4a, the ELF shows, as expected, two shells of electron localization, one for each atom, another enclosing the whole domain of the cluster. Within the domain of the cluster, we see that the ELF stays between 0.25 and 0.75 across most of its volume. In Fig. 3b the HOMO of the (b) structure is highly bipolar: the orbital has a heavy s component, what implies a stronger electron localization. A close inspection of the ELF in Fig. 4c–e, reveals that inside the cluster domain shell, there is a relatively large region whose ELF value drops below 0.25. These plots show how the electrons are more delocalized in the 2D structure than in the 3D one, hence explaining why the XC term favors the 2D structure over the 3D ones. The other 2D (HOMO in Fig. 3c and ELF in Fig. 4b) and 3D (HOMO in Fig. 3d and ELF in Fig. 4f–h) structures follow these trends: Fig. 3b orbital has a higher *s* component than Fig. 3a, as it can be seen from the relatively large lobes, but it is still highly *d*, hence the delocalization will be higher than Fig. 3c. Figure 3d on the other hand is another *s*-predominant, localized orbital.

The DOS depicted in Fig. 5, shows that the *s*–*d* hybridization is greater for Au clusters than for Ag ones, due to the *s*–*d* orbitals spatially overlapping more in Au (outer orbitals in Au are larger than Ag ones, while interatomic distance with first neighbors is close to the value for Ag clusters). This case is analogous to the findings of Grönbeck et al. [10] for Au and Cu. The analysis of the DOS graphics show a low component of S orbital in the HOMO for the 2D clusters while it is very large for the 3D ones, due to their higher sphericity. This is the origin of the kinetic energy term favoring 3D structures. It is to be noted that the *d* bands are very

[1] It is to be noted that ELF value interpretation sometimes presents problems: a notable case is the H_2 molecule, case in which we find ELF = 1 for all space.

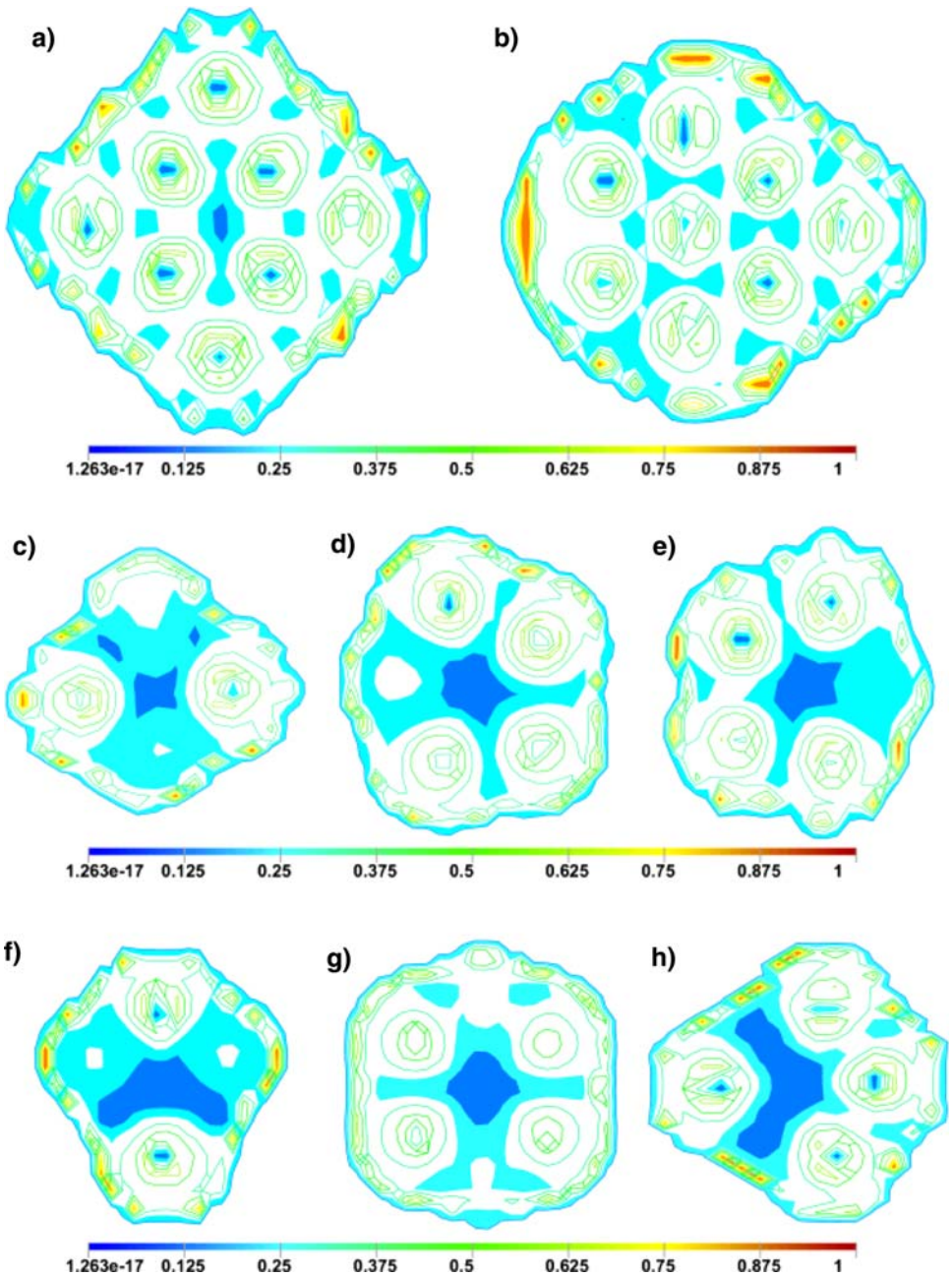

Fig. 4 The electron localization function (ELF) is plotted for the four lowest energy structures of the 8-atom Au cluster. **a** and **b** are the ELF on the plane *Z* of the Fig. 1**a** and **c** clusters, respectively. It is to be noted that *Z* is the plane where all the atoms are contained in both these clusters. **c**–**e** are, respectively, the ELF in the planes *X*, *Y*, *Z* of the Fig. 1**b** structure. **f**–**h** are, respectively, the ELF in the planes *X*, *Y*, *Z* of Fig. 1**d**. We have shaded the area where ELF drops below 0.25 or rises over 0.75, and a darker shade for where ELF drops below 0.125, or rises over 0.875. ELF takes values between 0 and 1

narrow in the (a) structure, due to its highly symmetric geometry. This slim width is obvious when analyzing the components of *d*: d_{zz}, d_{xz} and d_{yz} are dominant. Even though the (c) structure is regular, we do not see it in the *d* bands. But splitting it into its components we see that each one of them creates narrow bands. The distorted structures (b) and (d) have a very wide *d* band instead. The density matrix analysis of the Au clusters finds the HOMO orbital of (a) structure to be 0.99*d* and (c) structure to be 0.40*s*/0.39*p*/0.20*d*, while the (b) structure is 0.80*s*/0.20*d* and the (d) one is 0.74*s*/0.26*d*. The HOMO orbital of Ag clusters is, for (b) structure 0.72*s*/0.28*p*, for the (i) structure 0.63*s*/0.37*p*. The heavy s–$d_{z(x,y,z)}$ hybridization in the 3D Au clusters, compared to the *s*–*p* hybridization for their Ag counterparts, is what drives the former ones to inflated, more planar-like structures, due to the shape of the hybridized orbital [9].

5 Analysis and conclusions

Is there a relationship between the structural deformations of the 3D clusters with the fact that 2D clusters are energetically much more favored in Au than in Ag and Cu? From the results of our own research and other works [9, 30] we know that the minimum energy structures for Au

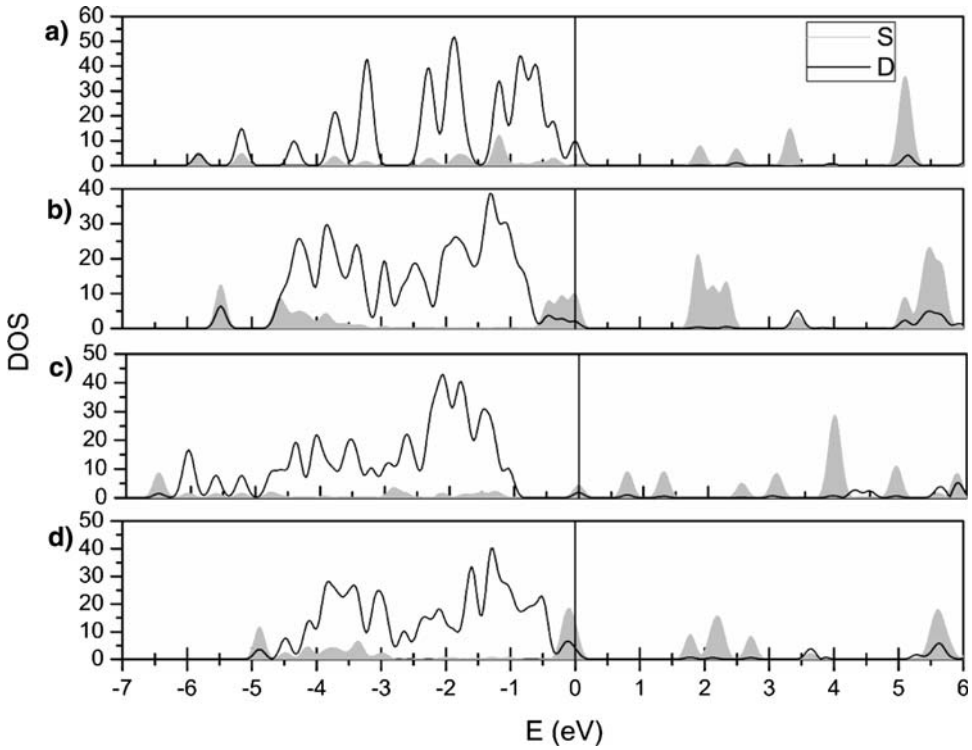

Fig. 5 The partial density of states (pDOS) of the types-S and -D orbitals are plotted for the four lowest energy structures of the 8-atom Au cluster. **a–d** are the pDOS of the **a–d** structures of Fig. 1, respectively. The origin of energies is placed in the energy of the highest occupied molecular orbital in each case

and Ag have a very small difference when considering the average distance between nearest neighbors (within 1%), and these distances are sensibly higher for them than for Cu. This reduced size is well known to be due to relativistic effects [16, 32]. This relativistic shortening of the size of the Au clusters increases the classical Coulomb repulsion among the Au nuclei and among the electrons of the cluster, hence favoring structures where the average distance between atoms is larger. The two-dimensional structures have a larger average distance between atoms even if the average distance between first neighbors is smaller, because the coordination number is lower. It has been observed for larger Au clusters (from 20 to 50 atoms) that while they are 3D, their lowest energy structure is not pseudo-close-packed, but instead, they tend to form cage-like structures. We have found that this is the case too even for clusters as small as 8 atoms, considering only their 3D structures, as current literature only finds regular 3D isomers. We can observe in Fig. 1 and Table 1 that the 3D clusters deform in a way that reduces the coordination number, and create "cavities" in their inside. The apparition of these cavities causes the ELF value to drop in them, as the electron density in those regions decreases respect to the rest of the volume. This makes the electrons in the 2D clusters to be more delocalized across their volume than in the 3D ones making the E_{XC} factor to be favorable to them (which, as we have seen, is the decisive energetic factor), stabilizing planar structures. Our results conflict with past works on this topic that shift the control of the dimensionality to the E_K term [10, 16] They do not find E_{XC} to play a significative role in the dimensionality of Au clusters, though they find it for Cu. In their studies they find that the E_K favors 2D structures because of the importance of *d–d* interaction. We have found in our calculations that this *d–d* overlapping is instead slightly larger in the 3D clusters, hence the E_K will be lowered for them. The orbital interaction that contributes to planarity is the important $s–d_{z(x,y,z)}$ hybridization; it helps stabilizing 2D structures, and destabilize regular 3D structures into more cage-like ones, making them have a larger E_{XC}. In Ref. [8] the 8-atom Au cluster is studied in comparison with the 8-atom Cu one. While they find the E_{XC} to control the dimensionality of the Cu clusters, they did not retrieve this behavior for the Au case. We have shown that for Au, and Ag too, the E_{XC} is still the energy term that controls the cluster dimensionality, hence we retrieve the same case for the three isoelectronic metals.

To summarize, we can conclude that the E_{XC} is an important factor to make the planar structures more competitive energetically. The *e–e* repulsion and the $s–d_{z(x,y,z)}$ hybridization slightly distort the 3D structures, which in turn, makes their E_{XC} larger. This is verified by the ELF.

Acknowledgments We wish to thank the help of the Centro de Supercomputación de Galicia (CESGA) for providing both computational resources and the technical support necessary for this research. Our work was supported by the Spanish Ministerio de Educación y Ciencia under the Project. No. MAT2006-10027. We also want to thank the program Isabel Barreto.

Appendix

From the original Becke and Edgecombe's definition of ELF (see footnote 1) we have that, for open-shell atomic systems:

ELF $= \frac{1}{1+\chi}$ with $\chi = \frac{\tau_\sigma - \frac{1}{4}\frac{(\nabla\rho_\sigma)^2}{\rho_\sigma}}{2^{\frac{5}{3}}C_F\rho_\sigma^{\frac{5}{3}}} = \frac{\sum_i^\sigma |\nabla\psi_i|^2 - \frac{1}{4}\frac{(\nabla\rho_\sigma)^2}{\rho_\sigma}}{2^{\frac{5}{3}}C_F\rho_\sigma^{\frac{5}{3}}}$ where τ_σ is the kinetic energy density for the σ-spin, ρ_σ is the electron density for the σ-spin and C_F is the Fermi constant, as in Ref. [33].

For closed-shell atoms: $\tau_\sigma = \frac{1}{2}\tau = \frac{1}{2}\sum_i^n |\nabla\psi_i|^2$.

Using the virial theorem for XC $E_{XC}[\rho]$ and kinetic energy $T_S[\rho]$ functionals from Levy and Perdew [34]:

$$E_X[\rho] = -\int \rho(\vec{r})\vec{r}\nabla\left(\frac{\partial E_X}{\partial\rho}\right)d\vec{r}$$

$$T_S[\rho] = -\frac{1}{2}\int \rho(\vec{r})\vec{r}\nabla\left(\frac{\partial T_S}{\partial\rho}\right)d\vec{r}$$

with Fuentealba's approximation [34]: $T_S[\rho] = -\frac{1}{2}E_X[\rho] - \frac{1}{2}\int\rho(\vec{r})\vec{r}\nabla\phi(\vec{r})d^3r - \frac{1}{2}T_C[\rho]$ where $\phi(\vec{r}) = \frac{Z}{r} - \int\frac{\rho(\vec{r})}{(\vec{r}-\vec{r}')}d^3\vec{r}'$ and T_C is the kinetic part of the correlation energy.

Since $E_{XC}[\rho] = E_X[\rho] + E_C[\rho]$ and having in account that $E_X[\rho] \gg E_C[\rho]$, and from Levy and Perdew [34]: $T_C = -E_C$, T_S can be approximated as:

$$T_S[\rho] = -\frac{1}{2}E_X[\rho] - \frac{1}{2}\int\rho(\vec{r})\vec{r}\nabla\phi(\vec{r})d^3r$$

By definition: $T_S[\rho] = \int t_S(\rho)d^3r$ and $T_S[\rho] = -\frac{1}{2}\int\nabla_r^2\gamma_S(r,r')\big|_{r'=r}d^3r$ where $\gamma_S(r,r')$ and where is the first-order reduced density matrix.

From this, as seen in Fuentealba's work [36], we have: $t_S(\rho) = \frac{1}{2}\sum_{i=1}^n|\nabla\psi_i(r')|^2 - \frac{1}{4}\nabla^2\rho(r)$ hence $\tau_\sigma = \frac{1}{2}\sum_{i=1}^n|\nabla\psi_i(r')|^2 = -\frac{1}{2}e_x - \frac{1}{2}\rho(r)\vec{r}\nabla\phi(r) + \frac{1}{4}\nabla^2\rho(r)$.

So, ELF approximated form is:

$$\text{ELF} = \left(1 + \frac{-\frac{1}{2}e_x - \frac{1}{2}\rho(r)\vec{r}\nabla\phi(r) + \frac{1}{4}\nabla^2\rho(r) - \frac{1}{4}\frac{(\nabla\rho_\sigma)^2}{\rho_\sigma}}{2^{\frac{5}{3}}C_F\rho_\sigma^{\frac{5}{3}}}\right)^{-1}$$

expression from which we take the dependence between XC energy and localization.

References

1. Mohan PJ, Datta A, Mallajosyula SS, Pati SK (2006) J Phys Chem B 110:18661. doi:10.1021/jp0639041
2. Wang SY, Yu JZ, Mizuseki H, Sun Q, Wang CY, Kawazoe Y (2004) Phys Rev B B 70:165413. doi:10.1103/PhysRevB.70.165413
3. López-Lozano X, Pérez LA, Garzón IL (2006) Phys Rev Lett 97:233401. doi:10.1103/PhysRevLett.97.233401
4. Heiz U, Bullock EL (2004) J Mater Chem 14:564. doi:10.1039/b313560h
5. Haruta M (2004) J New Mat Electrochem Syst 7:163
6. Nolan SP (2007) Nature 445:496. doi:10.1038/445496a
7. Majumder C, Briere T, Muzuseki H, Kawazoe Y (2002) J Chem Phys 117:7669. doi:10.1063/1.1509053
8. Majumder C, Kulshreshtha SK (2006) Phys Rev B 73:155427. doi:10.1103/PhysRevB.73.155427
9. Fernández EM, Soler JM, Garzón IL, Balbás LC (2004) Phys Rev B 70:165403. doi:10.1103/PhysRevB.70.165403
10. Grönbeck H, Broqvist P (2005) Phys Rev B 71:73408. doi:10.1103/PhysRevB.71.073408
11. Häkkinen H, Landman U (2000) Phys Rev B 62:R2287. doi:10.1103/PhysRevB.62.R2287
12. Fa W, Luo C, Dong J (2005) Phys Rev B 72:205428. doi:10.1103/PhysRevB.72.205428
13. Furche F, Ahlrichs R, Weis P, Jacob C, Gilb S, Bierweiler T, Kappes MM (2002) J Chem Phys 117:6982. doi:10.1063/1.1507582
14. Olson RM, Gordon MS (2007) J Chem Phys 126:214310. doi:10.1063/1.2743005
15. Bravo-Pérez G, Garzón IL, Novaro O (1999) Theochem. J Mol Struct 493:225
16. Häkkinen H, Moseler M, Landman U (2002) Phys Rev Lett 89:33401. doi:10.1103/PhysRevLett.89.033401
17. Zhao J, Yang J, Hou JG (2003) Phys Rev B 67:85404. doi:10.1103/PhysRevB.67.085404
18. St-Amant A, Salahub DR (1990) Chem Phys Lett 169:387. doi:10.1016/0009-2614(90)87064-X
19. Perdew JP, Wang Y, Engel E (1991) Phys Rev Lett 66:508. doi:10.1103/PhysRevLett.66.508
20. Pereiro M, Baldomir D, Iglesias M, Rosales C, Castro M (2001) Int J Quantum Chem 81:422 10.1002/1097-461X(2001)81:6<422::AID-QUA1011>3.0.CO;2-Z
21. Yabana K, Bertsch GF (1999) Phys Rev A 60:3809. doi:10.1103/PhysRevA.60.3809
22. Huzinaga S, Andzelm J, Kłbukowski M, Radzio-Andzelm E, Sakai Y, Tatewaki H (1984) Gaussian basis sets for molecular calculations. Elsevier, Amsterdam
23. Godbout N, Salahub DR, Andzelm J, Wimmer E (1992) Can J Chem 70:560. doi:10.1139/v92-079
24. Andzelm J, Radzio E, Salahub DR (1985) J Chem Phys 83:4573. doi:10.1063/1.449027
25. Schlegel HB (1995) Modern electronic structure theory. Word Scientific, Singapore, p 459
26. Diefenbach M, Kim KSJ (2006) Phys Chem B 110:21639. doi:10.1021/jp0649854
27. Bulusu S, Zeng XC (2006) J Chem Phys 125:154303. doi:10.1063/1.2352755
28. Xing X, Yoon B, Landman U, Parks JH (2006) Phys Rev B 74:165423. doi:10.1103/PhysRevB.74.165423
29. Tian D, Zhao J, Wang B, King RBJ (2007) Phys Chem A 111:411. doi:10.1021/jp066272r
30. Pereiro M, Baldomir D (2005) Phys Rev A 72:45201. doi:10.1103/PhysRevA.72.045201
31. Becke AD, Edgecombe KE (1990) J Chem Phys 92:5397. doi:10.1063/1.458517
32. Pyykkö P (1988) Chem Rev 88:563. doi:10.1021/cr00085a006
33. Kohout M, Savin A (1996) Int J Quantum Chem 60:875. doi:10.1002/(SICI)1097-461X(1996)60:4<875::AID-QUA10>3.0.CO;2-4
34. Levy M, Perdew JP (1985) Phys Rev A 32:2010. doi:10.1103/PhysRevA.32.2010
35. Fuentealba P (1997) J Phys At Mol Opt Phys 30:2039. doi:10.1088/0953-4075/30/9/007
36. Fuentealba P (1998) Int J Quantum Chem 69:559. doi:10.1002/(SICI)1097-461X(1998)69:4<559::AID-QUA13>3.0.CO;2-V